Nanoscale

COMMUNICATION

View Article Online
View Journal | View Issue

Cite this: *Nanoscale*, 2026, **18**, 8025

Received 21st November 2025,
Accepted 9th March 2026

DOI: 10.1039/d5nr04923g

rsc.li/nanoscale

(Sub-)microscale structuring of cellulose thin films using a polymer brush-assisted microcontact printing (PolyBrushMiC) routine

Nazim Pallab,[a,b] Maurice Schmette,[a,b] Sergio Kogikoski, Jr.,[a] Kay Hettrich,[b] Matthias Schenderlein[b] and Martin Reifarth *[a,b]

We present a method for directly (sub-)micropatterning cellulose thin films using microcontact printing with a polymer-brush stamp that carries reactive imidazole groups. These groups temporarily bind carboxylic-acid inks, enabling clean ester-forming transfer to cellulose without smearing, allowing high-resolution micro- or nanometre-scale chemical patterning for functional paper fabrication in a simple and efficient fabrication process.

Microcontact printing (μCP) is a soft lithography technique for (sub-)microscale surface patterning.[1] This cost-effective, quick, and simple technique can be used to transfer functional patterns of reactive chemical moieties onto a variety of substrates for the fabrication of micro-structured surfaces with a high spatial resolution. μCP uses a patterned elastomeric stamp that is functionalized with small or macromolecular compounds in order to transfer the patterns from the stamp surface to the substrate by establishing direct contact between them.[2–4] Many application fields such as sensing,[5,6] microelectronics,[7] tissue engineering,[8,9] information storage,[10] *etc.* benefit from μCP, making this method a versatile and facile technique. Compared to other patterning techniques, such as photopatterning,[11] dip pen lithography,[12] electron beam (e-beam) lithography,[13] and others, μCP does not rely on expensive instrumentation. Conventionally, μCP is conducted on plain smooth surfaces such as Au,[14,15] Si,[16] Cu,[17] Ag,[18] *etc.*, where usually high printing resolutions are achieved. Capillary-active or hydrophilic substrates, however, are challenging. At these interfaces, the ink tends to smear, which drastically limits the printing resolution of the process.[19,20] To address this issue, we have recently demonstrated a PolyBrushMiC method to directly pattern oxide and soft hydrogel surfaces precisely.[20–24]

In present day relevance, the μCP method can be utilized for selective addition of functional features onto sophisticated and demanding biocompatible and biodegradable surfaces.[25–27] Cellulose, being the most abundant biomolecule, is currently at the forefront of building functional materials.[28] This polysaccharide is composed of D-glucose being connected with 1,4-β-glycosidic bonds and has found abundant applications due to its non-toxicity, renewability, high surface area, adaptable physical, chemical, and mechanical properties, *etc.*[29] For chemical modification, the accessible hydroxy (*–OH*) groups of cellulose can be targeted for etherification,[30] esterification,[31–34] halogenation,[35] amination,[36] *etc.*, which transform cellulose into functional materials applicable in various fields such as water purification,[37] pharmaceuticals,[38] textiles,[39] coatings,[40] and packaging,[41] among many others. Among those, cellulose-based papers have gained attention as they can be chemically modified for multifaceted applications in making sensors, energy storage devices, green packaging, and many others.[42,43] Micro- or nano-patterning of such cellulose surfaces, therefore, would be valuable for generating structured and functionalized surfaces.[42,44] Surface patterning of cellulose has largely been carried out through different techniques such as embossing,[45] molding,[46] laser cutting,[47] and lithography techniques,[44,48–50] which are typically resolution-limited or require intensive equipment.[11] In contrast, a facile method like μCP has also been employed to introduce grafted patterns of linear polyethyleneimine (PEI)[51] and gold (Au)[52] on cellulose films and cellulose paper respectively. However, direct chemical patterning to functionalize cellulose surfaces has not been achieved yet. In this study, we tackle this issue and present the PolyBrushMiC strategy for the direct microscale transfer of chemical patterns onto cellulose thin films. With the approach reported here, cellulose is functionalized with activated carboxylic acids serving as inks, which form carboxylic ester bonds with the hydroxy functions present at the cellulose surface. Specifically, a patterned polydimethylsiloxane (PDMS) stamp is coated with a histamine-derived copolymer, to which the carboxylate inks are immobilized as

[a]*Institute of Chemistry, University of Potsdam, Karl-Liebknecht-Straße 24-25, 14476 Potsdam, Germany. E-mail: martin.reifarth@uni-potsdam.de*
[b]*Fraunhofer Institute for Applied Polymer Research, Geiselbergstraße 69, 14476 Potsdam, Germany*

N-acyl imidazoles. Subsequent transfer onto cellulose thin films occurs *via* imidazole-mediated esterification, producing well-defined microscale patterns at the cellulose surface. This technique offers a straightforward route to fabricating highly functional micropatterned cellulose materials.

Cellulose can be esterified using carboxylic acids. For their activation, the acids can first be converted to *N*-acyl imidazole intermediates, *e.g.,* by reaction with imidazole derivatives, such as 1,1'-carbonyl diimidazole (CDI). These intermediates can then transfer the acyl group to cellulose, yielding the corresponding esters.[33,53] This chemistry is effectively harnessed in our described PolyBrushMiC routine (Scheme 1). In the present protocol, an imidazole-functionalized copolymer – poly(90% di(ethyleneglycol)methylether methacrylate-*co*-10% histamine methacrylamide), referred to as poly(DEGMA-*co*-HMAm) – is grafted from a patterned PDMS stamp to immobilize carboxylic acids serving as an ink as *N*-acyl imidazole. For this purpose, the acyl inks are introduced as acid chlorides into the stamp-bound polymers. These ink patterns are subsequently transferred onto cellulose thin films by direct contact in the presence of an organic solvent. Syntheses are illustrated in Fig. S1–S4.

To provide a proof of principle of the transfer chemistry (Scheme 1), we started investigating the imidazole-mediated acyl transfer to a saccharide. Specifically, we used *N*-acetyl imidazole (Fig. S5) and selected it as a model compound resembling the histamine moiety of our grafted polymer. As a counterpart, phenyl-β-D-glucopyranoside was selected as a cellulose mimic, possessing free –OH groups and a protected anomeric carbon in its structure. An excess of *N*-acetyl imidazole was dissolved with the sugar in dimethyl sulfoxide (DMSO), and the reaction between the components in the mixture was allowed to proceed. Reaction progress is monitored by nuclear magnetic resonance (NMR) spectroscopy (Fig. S5 and S6). After complete solvent removal, the residue is analysed by ^{1}H and ^{13}C NMR. In the ^{1}H NMR spectrum, the appearance of singlet signals at approximately 2 ppm indicates a (partial) transfer of acetyl groups, which esterify the different hydroxy functions of the glucose molecule. However, full acetylation could not be achieved, as seen in Fig. S5.

After having demonstrated the successful acetyl group transfer from imidazole, we pursued the PolyBrushMiC technique. Our printing routine involves the fabrication of brush stamps as a first step. Accordingly, we use elastomeric PDMS stamps bearing grooves with 4 μm dimension, which we aimed to functionalize with poly(DEGMA-*co*-HMAm). HMAm is introduced as the monomeric unit for immobilization of the ink, while DEGMA is employed to mediate the solubility of the polymer without interfering with the inking process. The HMAm monomer synthesis is carried out according to the literature (Fig. S1 and S7–S9 show the syntheses and the characteristic spectra).[54] For grafting, the stamps are first activated *via* plasma treatment and subsequently functionalized with 3-aminopropyl triethoxysilane (APTES) and the chain transfer agent (CTA) 4-cyano-4-[[(dodecylthio)carbonothioyl]thio]pentanoic acid, resulting in CTA immobilization onto the stamp surface. In a next step, the polymer is grafted from the stamp's surface through the RAFT polymerization technique using a shuttled CTA approach, where additional CTA in solution usually facilitates controlled polymerization and chain transfer (Fig. 1a and b). Accordingly, during the polymerization process, excess shuttle CTA is present in solution so that polymer chains formed simultaneously at the stamp surface as well as in solution. Assuming similar chain growth kinetics, we were able to characterize the solution-phase polymers, being representative for the brush polymer chains.[22,55] The polymers are characterized accordingly *via* ^{1}H NMR and SEC (Fig. 1c), exhibiting an M_n of 101 000 g mol^{-1} (a degree of polymerization, DP, of 500 was targeted) with a dispersity index ($Đ$) value of 1.94. Other representative size exclusion chromatography (SEC) curves and related data of the polymer formed in the solution are included in Fig. S10 and Table S1. Despite the high dispersity of the polymer, indicative for a limited control over the polymerization process, the resulting brushes are nevertheless functional.

This finding aligns with our previous observations that surface-grafted brushes remain effective in PolyBrushMiC procedures despite limited polymerization control during their preparation.[20,21]

As an ink, we deploy a fluorescent label possessing a carboxylate, which could be converted into an acid chloride, maintaining its integrity. The ink is based on a 7-nitrobenzo-2-

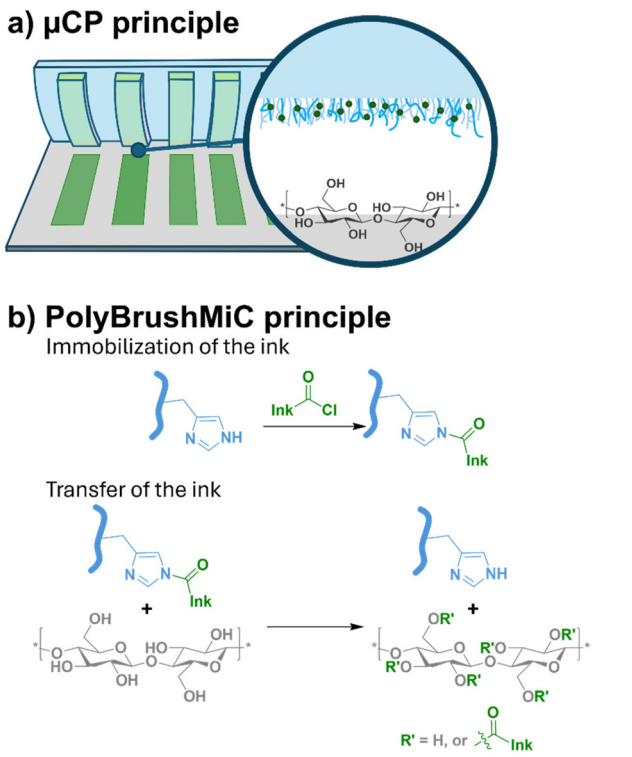

Scheme 1 (a) Schematic illustration of the overall μCP process. (b) Imidazole group of a grafted polymer containing histamine side-chains that binds the acyl ink molecule in the first step. In the subsequent step, the ink transfers from the polymer to the cellulose substrate, forming cellulose ester patterns at the surface.

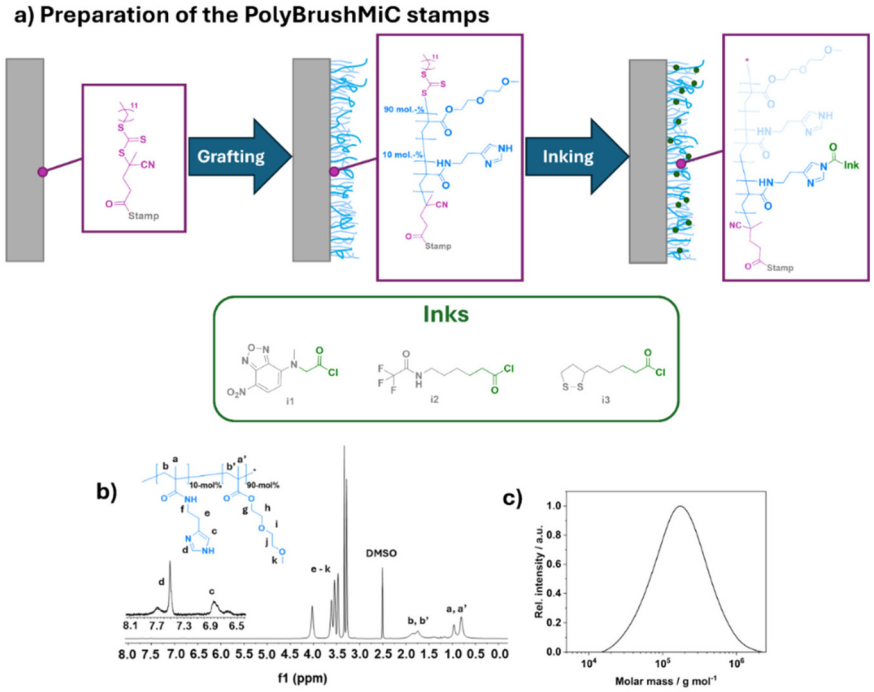

Fig. 1 Preparation of the stamp. (a) Schematic representation of stamp surface functionalization: a CTA attached stamp is used to graft polymer brushes from the surface, followed by inking in a three step-process. (b) and (c) ^{1}H NMR (DMSO-d_6) spectra and SEC (THF as an eluent, PS standard) plot of the formed polymer in the grafting solution of poly(DEGMA-*co*-HMAm) from the stamp surface (M_n = 101 000 g mol^{-1}, $Đ$ = 1.94).

oxa-1,3-diazole (NBD), which is generally known for its fluorescent characteristics and used for labelling functional molecules.[56] To prepare the fluorescent carboxylate dye, NBD is first conjugated with sarcosine (Fig. S2 and S11–S13), and its primary carboxylic acid group is next converted into an acyl chloride (**i1**, Fig. S14 and S15). In a subsequent step, the stamp is immersed in the inking solution (**i1**) to attach the ink to the imidazole moiety of HMAm (Fig. 1a). The inked stamp is then washed to remove any excess dye, which potentially also accumulated within the PDMS stamp network. Note that the stamp must be treated under strictly anhydrous conditions in view of its hydrolysis instability.

In a next step, we aimed to prepare a suitable cellulose surface acting as a substrate for μCP (Fig. 2a). Opting for the functionalization of papers, we use a nanometre-thick cellulose film as a model substrates.[57] For this purpose, we start from cellulose pulps, which are first dissolved in a mixture of lithium chloride and *N*,*N*′-dimethyl acetamide (LiCl/DMAc) to prepare a dilute solution of cellulose.[58] Thin films of cellulose are prepared by sequential spin coating of a 1% aqueous solution of polyethyleneimine (PEI) followed by cellulose solution on clean Si wafers. The topology of the thin film surface was characterized *via* atomic force microscopy (AFM, Fig. 2b). In the corresponding images, clearly a fibrous morphology of the surface can be observed, possessing a layer thickness of approx. 70 nm (Fig. S16).

Further characterization of the cellulose thin films was conducted with Fourier-transform infrared (FTIR) spectroscopy. The characteristic functional group signals, namely O–H stretching

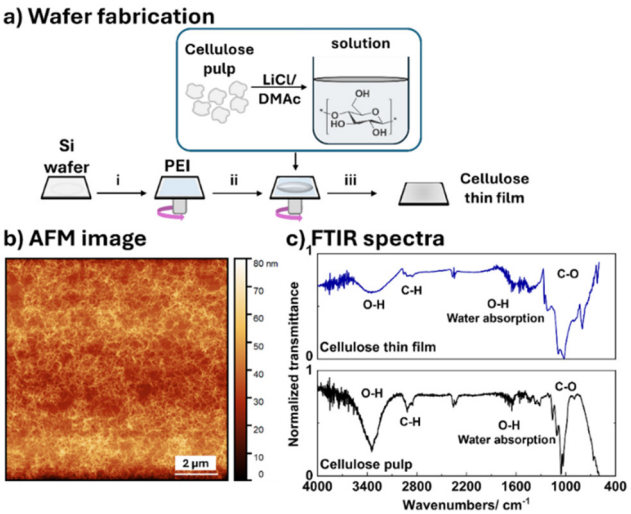

Fig. 2 Substrate preparation. (a) Illustration of cellulose thin film formation procedures on a Si wafer. The cleaned Si wafer was spin coated with polyethyleneimine (PEI) and cellulose solution respectively. The wafer was then washed and dried. (b) AFM topography image of the cellulose film on the Si wafer. (c) FTIR spectra of the cellulose pulp and cellulose thin film showing the presence of functional groups of native cellulose.

(~3400 cm^{-1}), C–H stretching (2900 cm^{-1}), O–H bending from water absorption (1647 cm^{-1}), and C–O–C pyranose ring vibration (1050 cm^{-1}) bands, are observed, being indicative of cellulose (Fig. 2c) as described in the literature.[59] At the same

time, FTIR spectroscopy was conducted on the cellulose pulp, where the same set of signals is found (FTIR signals measured for the background and a clean Si wafer as controls are shown in Fig. S17). Overall, these findings clearly indicate that a cellulose film is successfully added to the Si wafer.

After substrate fabrication, we carried out the printing experiments. Supporting spectra characterising additional synthesis products are given in Fig. S18–S27. Note that it is essential during the printing process to ensure the absence of moisture in the substrate. To avoid hydrolysis as a severe competing reaction to the esterification, excessive drying of the substrate is mandatory. For the subsequent printing process, we first inked the stamp. Accordingly, we took a grafted stamp and exposed it to the NBD-sarcosine acid chloride (**i1**). In search of an appropriate aprotic solvent for the inking reaction that does not interfere with acyl imidazole, we utilise dichloromethane (DCM). The inked stamp is next used to transfer **i1** fluorescent dye to the cellulose substrate. The stamp and the substrate, for this purpose, are both immersed in dry DMSO in a custom-made printing chamber, thereby avoiding exposure to moisture. The printing chamber was prepared by Fused Deposition Modelling (FDM) 3D printing (Fig. S28).

After a printing time of 40 minutes, the substrate is investigated. As shown in Fig. 3a, the substrate clearly shows the signature of the stamp, *i.e.* regular stripe patterns with a size of 4 μm, that were transferred as fluorescent areas to the cellulose thin film.

To highlight the necessity of the PolyBrushMiC strategy, we conducted negative control experiments using unmodified (bare) stamps. As the ink, a solution of the *N*-acyl imidazole derivative of NBD-sarcosine is prepared, which was generated *in situ* by adding imidazole to the acid chloride, since the imidazole derivatives possess controlled reactivity. For the inking step, a stamp is immersed in this solution overnight. As shown in Fig. 3b, smeared and low-resolution patterns are transferred onto the substrate, which can be explained by significant diffusive distribution of the ink molecules at the substrate using low molecular-weight ink, *i.e.* ink smearing undermining a good printing resolution. This result indicates that the PolyBrushMiC strategy is indispensable to achieve a printing resolution that is sufficient. As an additional experiment, we also performed printing with a bare stamp using the acid chloride directly as the ink. No patterns are observed (Fig. 3c), likely due to the excessive reactivity of the acid chloride, which might have led to compound degradation. Adsorbing dye molecules, being transferred by this process, could efficiently be removed by subsequent washing steps.

Having pointed out the necessity for the imidazole-mediated PolyBrushMiC strategy, we next wanted to examine this process in more detail. In order to obtain an insight into the kinetics of the transfer process, printing was carried out for different durations (10, 20, 40, 60, and 120 min, Fig. S29a). A plot of the normalized fluorescence intensity against the pattern distance (Fig. S29b) indicates that accurate and precise transfer occurred after 40 min. Varying the printing time, whether shorter or longer, resulted in reduced pattern resolution. While at shorter printing times, too few ink molecules were transferred to the surface, leading to weak pattern formation, and the reduced printing quality observed at longer durations appeared at first glance surprising. However, we explain the reduced pattern quality at higher printing durations by increased cellulose functionalization over time. Greater functionalization enhances the solubility of the cellulose surface layer in DMSO, which is used as the solvent during transfer. As a result, the highly functionalized upper layer becomes more prone to dissolution, resulting in partial removal. In this context, acetonitrile (ACN), another polar aprotic solvent, was also successfully employed for the printing process. While well-defined patterns could be obtained in the presence of ACN (Fig. S30), the accuracy is slightly decreased compared to that achieved using DMSO. As indicated in Scheme 1, the polymer-bound imidazole is regenerated after ink transfer, in principle allowing for multiple uses. Based on this concept, we anticipated that the stamp would be re-usable. To test this, a single stamp is deployed for multiple printing cycles – up to four – on cellulose films. As shown in

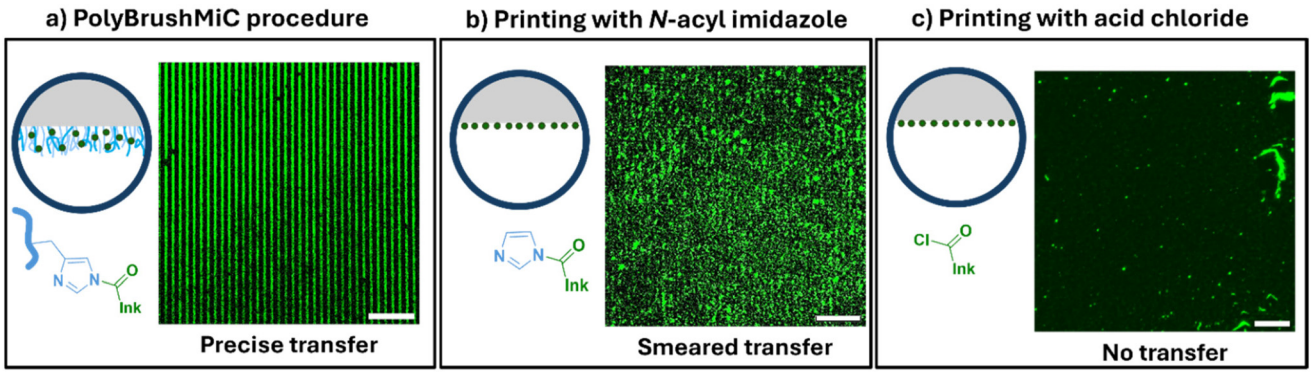

Fig. 3 Microcontact printing results. (a) Fluorescence microscopy image of the NBD-sarcosine acyl chloride (**i1**) printed substrate from a grafted stamp showing accurate patterns, and (b) printed substrate with a bare stamp, using the ink-functionalized *N*-acyl imidazole. The printing process results in smeared patterns. (c) Printed substrate with a bare stamp, using the mere ink carboxylic acid chloride. The process does not result in the formation of visible patterns. Scale bars are 20 μm.

Fig. S31, the stamp could indeed be reused for several printing processes. However, the resolution of the printed patterns noticeably declined after the third and fourth uses, suggesting a gradual loss of polymer integrity.

We attribute this degradation to the aggressive nature of the acid chloride, which releases HCl and likely causes partial disintegration of both the PDMS stamp and the polymer brush. Hydrolysis reactions can generate non-reactive dye species that may still physically adsorb onto the printed areas. However, since no patterns are observed after washing, these adsorbed dyes are likely removed during the washing step. In contrast, the printed areas that remained intact after washing indicate that the dyes are covalently attached and therefore cannot be removed.

Although the synthesis of acyl chlorides is relatively straightforward and cheap, their high reactivity can impose practical limitations, such as degradation or swelling of the PDMS stamp due to their harsh chemical nature. To overcome these constraints, less aggressive acid anhydrides were also explored as alternative ink molecules. In this context, fluorescent NBD-sarcosine anhydride (**i1$_a$**) is synthesized *in situ* and employed for inking. Fluorescence microscopy revealed well-defined pattern formation, confirming successful transfer using the acid anhydride ink (Fig. S32).

To broaden the application range of PolyBrushMiC for patterning cellulose surfaces, a series of additional printing experiments is conducted. Accordingly, the rough side of a silicon wafer was coated with a thin cellulose film, resulting in a substrate with a mean roughness of approx. 220 nm (Fig. S33a and b). This substrate serves as a model system to mimic highly surface-rough papers. Due to the pronounced surface roughness and waviness of the substrate, the resulting patterns appear faded (Fig. S33c), as the stamp was unable to fully conform to the surface topography.

To estimate the resolution limit of the method, printing is performed using a monolayer of polymer brush-functionalized microspheres as microstamps that are pressed against a cellulose film (Fig. 34a). Specifically, the particles were first aligned in a PDMS support possessing grooves that matched the particle size (Fig. 34b) and subsequently grafted with poly (DEGMA-*co*-HMAm). The resulting printed features, originating from the contact areas between the polymer brush-functionalized microparticles aligned in the stamp and the cellulose surface, exhibit submicroscale dimensions with an average feature size of *ca.* 550 nm (Fig. S34c and d). Given the relatively large particle diameters employed in this simplified experiment, these dimensions suggest that ink transfer occurs predominantly within the actual contact area between the microstamp and the cellulose film, rather than being driven by diffusive spreading. A further explanation is provided in Fig. S35 and in the subsequent discussion.

This approach is further extended to replicate nanoscale patterns (*ca.* 250 to 750 nm) from the polycarbonate layer of a digital versatile/video disc (DVD, Fig. S36a–d, AFM and optical microscopy images). These patterns were transferred onto the cellulose substrate using the PolyBrushMiC strategy (Fig. S37). While complete pattern transfer is not achieved, optimization of the stamp material and processing parameters may enable more accurate and comprehensive replication in future studies. Overall, these results demonstrate the feasibility of reproducing submicroscale features and potentially storing such information on cellulose-based substrates such as paper. It is noteworthy that previous work from our group determined the polymer brush thickness to be approximately 20 nm,[21] a dimension unlikely to significantly compromise edge definition or induce substantial lateral ink diffusion at such a nanoscale, securing the pattern resolution when printed from the stamp.

Having demonstrated the possibility to introduce micro- and nanoscale patterns onto the cellulose substrates, we opted to elucidate the chemical nature of the binding in more detail. In order to obtain quantitative information about the printing process, we characterized the printing areas using X-ray photoelectron spectroscopy (XPS). As a probe, we use a fluorinated compound as ink (**i2**), as fluorine represents a chemical element with a characteristic XPS signature along with suitable sensitivity.[60,61] In this respect, we synthesized 6-(2,2,2-trifluoroacetamido)hexanoyl chloride (**i2**) from its respective acid to act as an XPS probe. The synthesis and all the NMR and mass spectra of the corresponding acid and acid chloride are shown in Fig. S3 and S18–S23. For analysis, a flat, non-structured stamp is inked in the aforementioned acyl chloride (**i2**) and washed with dry DCM. After careful drying of the stamp, the ink is transferred onto cellulose thin films. XPS confirms the successful transfer of ink by the presence of a distinct F 1s signal at 688–689 eV (Fig. 4a), attributable to the organic fluorine of the acyl chloride ink. The atomic concentration value obtained from XPS (Fig. 4b) revealed a fluorine content of 0.8 ± 0.4%. Furthermore, the carbon region exhibited a C–F signal at ~293 eV (Fig. S38a), being characteristic of a $-CF_3$ chemical environment.[60] The fluorine quantity can be compared with the carbon content to estimate the degree of functionalization (DF) of the cellulose unit. Approximately 40% out of the 60% measured carbon content can be attributed to cellulose, while most of the remaining carbon (%) likely originates from environmental contamination as indicated by pronounced C–C and C–H regions (~285 eV) observed in the C 1s spectra (Fig. S38b). Based on this estimation, a DF value of 1.4% per anhydro-glucose unit (AGU, representing the monomeric repeating unit) of cellulose can be calculated (over the detected sample volume; details are shown in the SI along with Fig. S38). For comparison, we conducted a negative experiment with a bare stamp (non-grafted, **i2**-inked) as well. μCP performed in such a way shows almost no transfer (Fig. S38b and c) in contrast to the printing with a grafted stamp.

To evaluate the binding chemistry of the acid-based ink more specifically, we characterized the resulting printing patterns using vibrational spectroscopy. For functionalization, lipoic acid is employed as an ink, enabling the anchoring of gold nanoparticles (AuNPs) to the printing patterns. Accordingly, we first synthesized α-lipoyl chloride (**i3**), which is subsequently used as an ink in the PolyBrushMiC process. The synthesis of **i3** followed established procedures from the literature (characterization studies in Fig. S4 and S24).[62]

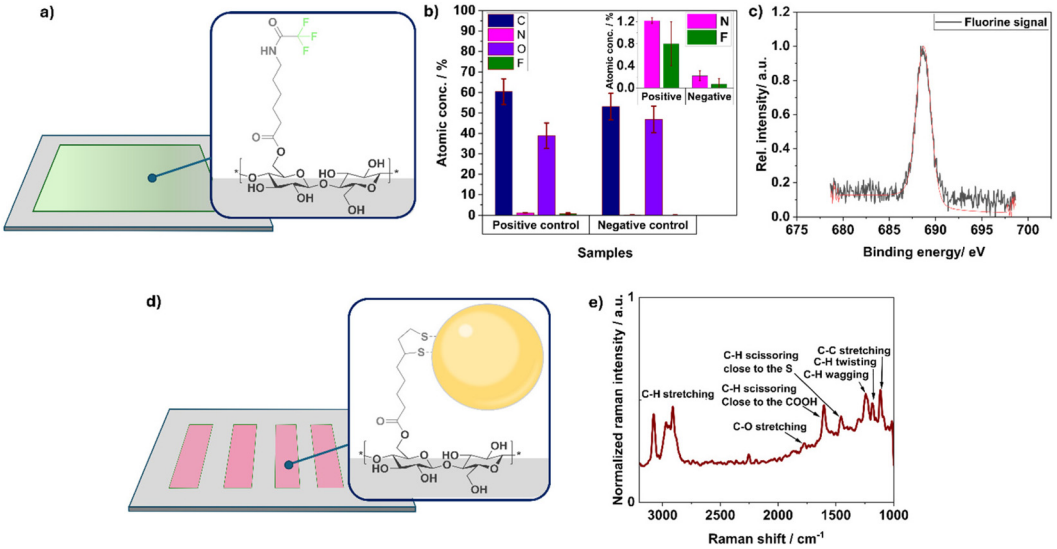

Fig. 4 (a) Illustration of a cellulose substrate functionalized with 6-(2,2,2-trifluoroacetamido)hexanoyl chloride (**i2**). (b) Atomic concentrations (%) calculated from XPS spectra along with (c) the high resolution F 1s XPS spectrum of the **i2** printed substrate. The inset of (b) shows zoomed-in atomic concentrations (%) of N and F contents. The presence of fluorine and other elements (positive control: C = 60 ± 6.28%, O = 39 ± 6.24%, N = 1.22 ± 0.05%, F = 0.8 ± 0.4%; negative control: C = 53 ± 6.51%, O = 47 ± 6.84%, N = 0.22 ± 0.09%, F = 0.07 ± 0.1%) indicates that printing with a grafted stamp transfers **i2** more effectively than printing with a bare stamp. (d) Schematic representation of the **i3** patterned cellulose substrate and Au NP deposition (0.05 mg ml^{-1}, 40 nm) on the surface. (e) Representative SERS spectra of AuNP-deposited patterned cellulose substrates. Different areas of the patterned substrate were analysed to observe the presence and absence of lipoic acid signals.

In the next step, the printed substrate is immersed in an aqueous dispersion of AuNPs (0.05 mg mL^{-1}, 40 nm diameter), which selectively bound to the patterned regions through sulfur–Au covalent bonding. Due to the presence of nanoparticles in the patterned areas, we expect that Raman signals from molecules in the vicinity of the AuNP surface will be enhanced, giving rise to surface-enhanced Raman spectroscopy (SERS) signals.

We mapped a distinct patterned region exhibiting SERS-enhanced Raman signals, which are attributed to lipoic acid in proximity to the AuNP (Fig. 4e). The obtained spectra show characteristic vibrational bands of lipoic acid,[63] including C–C stretching at 1116 cm^{-1}, C–H twisting and C–H wagging at 1185 and 1240 cm^{-1}, and C–H scissoring at 1460 and 1600 cm^{-1}; with the latter being very enhanced and most likely correlated with C–H closer to the nanoparticle surface. A small band at 1770 cm^{-1} is assigned to the C–O stretching. Additionally, a set of bands in the region near 3000 cm^{-1} are associated with different coupled C–H stretches. These findings are clearly indicative for the attachment of **i3** to the cellulose surface. In contrast, non-patterned regions showed no such signals (Fig. S39), as expected for mere cellulose samples. To further validate the covalent interaction between the NPs and the patterned area, SERS spectra were recorded for a pristine cellulose-coated substrate and for a cellulose-coated substrate deposited with AuNPs, and these are compared to the spectrum of the particle-deposited printed surface. The lipoic acid-modified substrate exhibits signals corresponding to those regions observed in the patterned area, whereas the two control substrates show no significant characteristic peaks (Fig. S40). This indicates that AuNPs deposited on a bare cellulose wafer show no covalent attachment of NPs, unlike the lipoic acid functionalized substrate. Note that minor shifts or slight deviations in the characteristic lipoic acid bands can likely be attributed to the ultrathin film thickness and the relatively low surface concentration of lipoic acid.

In summary, we introduce a polymer-assisted μCP strategy for the direct patterning of cellulose surfaces. Well-defined cellulose ester patterns are generated by transferring acyl groups from an imidazole-containing poly(DEGMA-*co*-HMAm) brush to cellulose thin films. Three types of acyl chlorides are employed as inks: a fluorescent dye for microscopy visualization, a fluorinated acid as an XPS probe, and a disulfide-containing acid enabling SERS detection. These inks are immobilized onto polymer chains grafted from elastomeric PDMS stamps and subsequently transferred to cellulose films through imidazole-mediated esterification. Ink transfer is validated by complementary analytical techniques, with fluorescence microscopy in particular confirming the precise deposition of a fluorescent dye in stripe patterns. This approach is broadly applicable, as both the grafted polymer and the substrate can be tailored, establishing μCP as a versatile platform for direct patterning and selective functionalization of cellulose surfaces, with potential extension to cellulose-based papers.

Author contributions

Nazim Pallab: conceptualization, validation, investigation, visualization, and writing – original draft. Maurice Schmette:

validation, investigation, and writing – review and editing. Sergio Kogikoski Jr.: investigation, data curation, and writing – review and editing. Kay Hettrich: investigation and writing – review and editing. Matthias Schenderlein: investigation, data curation, and writing – review and editing. Martin Reifarth: conceptualization, methodology, funding acquisition, supervision, visualization, and writing – review and editing.

Conflicts of interest

The authors declare no competing financial interest.

Data availability

The data supporting this article (spectra, chromatograms, microscopy images) have been included as part of the supplementary information (SI). Supplementary information is available. See DOI: https://doi.org/10.1039/d5nr04923g.

An earlier version of this article has been submitted to ChemRxiv.

Acknowledgements

The authors gratefully acknowledge Prof. Dr. Alexander Böker (Fraunhofer Institute for Applied Polymer Research, IAP, Potsdam) for his valuable support. N. P. and M. R. thank the German Research Foundation (DFG) for financial support under project number 471323994. M. R. and S. K. Jr. acknowledge funding by the DFG in the framework of the Collaborative Research Center (CRC) 1636 (project number 510943930, project B01). The authors further thank ZUMOLab GmbH (Wesseling, Germany) for providing the "ZUMO-MCP (Microcontact Printer)" used in this study. Stefan Langen from the University of Potsdam is gratefully acknowledged for his support with IR measurements. Additional support by the University Research Focus Sustainable Materials Design at the University of Potsdam is also gratefully acknowledged.

References

1 Y. Xia and G. M. Whitesides, *Annu. Rev. Mater. Sci.*, 1998, **28**, 153–184.
2 T. Kaufmann and B. J. Ravoo, *Polym. Chem.*, 2010, **1**, 371–387.
3 M. Reifarth, *Soft Matter*, 2025, **21**, 6658–6678.
4 L. Zhai, D. W. Laird and R. D. McCullough, *Langmuir*, 2003, **19**, 6492–6497.
5 C. A. Gunawan, M. Ge and C. Zhao, *Nat. Commun.*, 2014, **5**, 3744.
6 H.-J. Lim, D. Y. Lee and Y.-J. Oh, *Sens. Actuators, A*, 2006, **125**, 405–410.
7 L. Stolz Roman, O. Inganäs, T. Granlund, T. Nyberg, M. Svensson, M. R. Andersson and J. C. Hummelen, *Adv. Mater.*, 2000, **12**, 189–195.
8 M. Théry and M. Piel, *Micropatterning in cell biology*, Academic Press, Amsterdam, 2014.
9 R. Kane, *Biomaterials*, 1999, **20**, 2363–2376.
10 S. Han, Y. Zhou, Z. Xu, L. Huang, X. Yang and V. A. L. Roy, *Adv. Mater.*, 2012, **24**, 3556–3561.
11 M. J. Madou, *Fundamentals of Microfabrication*, CRC Press, 2018.
12 G. Liu, S. H. Petrosko, Z. Zheng and C. A. Mirkin, *Chem. Rev.*, 2020, **120**, 6009–6047.
13 T. Lohmüller, D. Aydin, M. Schwieder, C. Morhard, I. Louban, C. Pacholski and J. P. Spatz, *Biointerphases*, 2011, **6**, MR1–MR12.
14 A. Kumar and G. M. Whitesides, *Appl. Phys. Lett.*, 1993, **63**, 2002–2004.
15 J. C. Love, L. A. Estroff, J. K. Kriebel, R. G. Nuzzo and G. M. Whitesides, *Chem. Rev.*, 2005, **105**, 1103–1170.
16 J. Kim, N. Takama and B. Kim, *Sens. Mater.*, 2005, **17**, 49–56.
17 Y. Xia, E. Kim, M. Mrksich and G. M. Whitesides, *Chem. Mater.*, 1996, **8**, 601–603.
18 Y. Xia, N. Venkateswaran, D. Qin, J. Tien and G. M. Whitesides, *Langmuir*, 1998, **14**, 363–371.
19 A. Perl, D. N. Reinhoudt and J. Huskens, *Adv. Mater.*, 2009, **21**, 2257–2268.
20 N. Pallab, S. Reinicke, J. Gurke, R. Rihm, S. Kogikoski, M. Hartlieb and M. Reifarth, *Polym. Chem.*, 2024, **15**, 853–867.
21 P. Akarsu, R. Grobe, J. Nowaczyk, M. Hartlieb, S. Reinicke, A. Böker, M. Sperling and M. Reifarth, *ACS Appl. Polym. Mater.*, 2021, **3**, 2420–2431.
22 P. Akarsu, S. Reinicke, A. Lehnen, M. Bekir, A. Böker, M. Hartlieb and M. Reifarth, *Small*, 2023, 2301761.
23 M. Reifarth, M. Sperling, R. Grobe, P. Akarsu, F. Schmitt, M. Schmette, S. Tank, K. M. Arndt, S. Chiantia, M. Hartlieb and A. Böker, *Adv. Funct. Mater.*, 2025, **35**, 2423495.
24 N. Pallab, E. Sperlich, M. Schenderlein, A. Krüger-Genge, J. Li, L. Zeininger, Z. Tošner, M. Uchman and M. Reifarth, *Angew. Chem., Int. Ed.*, 2025, **64**, e202501759, (*Angew. Chem.*, 2025, **137**, e202501759).
25 A. G. Castaño, V. Hortigüela, A. Lagunas, C. Cortina, N. Montserrat, J. Samitier and E. Martínez, *RSC Adv.*, 2014, **4**, 29120–29123.
26 M. J. Poellmann, K. L. Barton, S. Mishra and A. J. W. Johnson, *Macromol. Biosci.*, 2011, **11**, 1164–1168.
27 M. Burek and I. Wandzik, *Polym. Rev.*, 2018, **58**, 537–586.
28 T. Aziz, W. Li, J. Zhu and B. Chen, *Int. J. Biol. Macromol.*, 2024, **278**, 134695.
29 E. Marinho, *Sustainable Chem. Environ.*, 2025, **11**, 100283.
30 J. You, X. Zhang, Q. Mi, J. Zhang, J. Wu and J. Zhang, *Cellulose*, 2022, **29**, 9583–9596.
31 Y. Wang, X. Wang, Y. Xie and K. Zhang, *Cellulose*, 2018, **25**, 3703–3731.

32 T. Heinze, T. Liebert and A. Koschella, *Esterification of Polysaccharides*, Springer-Verlag, Berlin-Heidelberg, 2006, ch. 9, pp. 169–180.
33 T. F. Liebert and T. Heinze, *Biomacromolecules*, 2005, **6**, 333–340.
34 D. Klemm, B. Philipp, T. Heinze, U. Heinze and W. Wagenknecht, *Comprehensive Cellulose Chemistry: Functionalization of Cellulose*, Wiley-VCH, Weinheim, 1998, vol. 2, pp. 99–164.
35 C. Gao, S. Liu and K. J. Edgar, *Carbohydr. Polym.*, 2018, **193**, 108–118.
36 S. Zhang, L. Liu, J. Yu and Y. Fan, *Ind. Crops Prod.*, 2024, **222**, 119500.
37 K. Bethke, S. Palantöken, V. Andrei, M. Roß, V. S. Raghuwanshi, F. Kettemann, K. Greis, T. T. K. Ingber, J. B. Stückrath, S. Valiyaveettil and K. Rademann, *Adv. Funct. Mater.*, 2018, **28**, 1800409.
38 H. C. Arca, L. I. Mosquera-Giraldo, V. Bi, D. Xu, L. S. Taylor and K. J. Edgar, *Biomacromolecules*, 2018, **19**, 2351–2376.
39 G. Nocca, A. Arcovito, N. A. Elkasabgy, M. Basha, N. Giacon, E. Mazzinelli, M. S. Abdel-Maksoud and R. Kamel, *Pharmaceutics*, 2023, **15**, 2738.
40 E. Palmieri, G. Giordanengo, M. Bonomo, V. Guglielmotti, L. Severini, C. Mazzuca, C. Barolo and S. Orlanducci, *ACS Appl. Polym. Mater.*, 2024, **6**, 11776–11787.
41 X. Liu, Z. Qin, Y. Ma, H. Liu and X. Wang, *J. Renewable Mater.*, 2023, **11**, 3203–3225.
42 F. Zhang, K. Xu, Y. Bai and P. Wang, *Cellulose*, 2023, **30**, 8539–8569.
43 M. Wang, Y. Wang, B. Gao, Y. Bian, X. Liu, Z. He, Y. Zeng, X. Du and Z. Gu, *ACS Appl. Mater. Interfaces*, 2019, **11**, 14445–14456.
44 Y. Zhou, Y. Li, F. Dundar, K. R. Carter and J. J. Watkins, *Cellulose*, 2018, **25**, 5185–5194.
45 Y.-J. Juang, P.-S. Chen and Y. Wang, *Sens. Actuators, B*, 2019, **283**, 87–92.
46 C. Browne, G. Garnier and W. Batchelor, *J. Colloid Interface Sci.*, 2021, **587**, 162–172.
47 M. A. Mahmud, E. J. M. Blondeel, M. Kaddoura and B. D. MacDonald, *Micromachines*, 2018, **9**, 220.
48 T. Ganner, J. Sattelkow, B. Rumpf, M. Eibinger, D. Reishofer, R. Winkler, B. Nidetzky, S. Spirk and H. Plank, *Sci. Rep.*, 2016, **6**, 32451.
49 A. Wolfberger, A. Petritz, A. Fian, J. Herka, V. Schmidt, B. Stadlober, R. Kargl, S. Spirk and T. Griesser, *Cellulose*, 2015, **22**, 717–727.
50 C. Browne, M. J. Hertaeg, D. J. Mendoza, M. Naseri, M. Lin, G. Garnier and W. Batchelor, *Colloids Surf., A*, 2023, **656**, 130379.
51 F. Kettling, B. Vonhören, J. A. Krings, S. Saito and B. J. Ravoo, *Chem. Commun.*, 2015, **51**, 1027–1030.
52 H. G. Lim, G. Y. Cho, J. Kim and K. S. Kang, *Sens. Actuators, A*, 2009, **153**, 131–135.
53 M. Beaumont, C. G. Otoni, B. D. Mattos, T. V. Koso, R. Abidnejad, B. Zhao, A. Kondor, A. W. T. King and O. J. Rojas, *Green Chem.*, 2021, **23**, 6966–6974.
54 J. Ji, X. Li, T. Wu and F. Feng, *Chem. Sci.*, 2018, **9**, 5816–5821.
55 Z. Zheng, J. Ling and A. H. E. Müller, *Macromol. Rapid Commun.*, 2014, **35**, 234–241.
56 S. Archer, F. Medzihradsky, A. Seyed-Mozaffari and P. J. Emmerson, *Biochem. Pharmacol.*, 1992, **43**, 301–306.
57 C. Aulin, S. Ahola, P. Josefsson, T. Nishino, Y. Hirose, M. Österberg and L. Wågberg, *Langmuir*, 2009, **25**, 7675–7685.
58 C. Achtel and T. Heinze, *Macromol. Chem. Phys.*, 2016, **217**, 2041–2048.
59 M. El-Sakhawy, S. Kamel, A. Salama and H.-A. S. Tohamy, *Cellul. Chem. Technol.*, 2018, **52**, 193–200.
60 C. Nietzold, P. M. Dietrich, S. Ivanov-Pankov, A. Lippitz, T. Gross, W. Weigel and W. E. S. Unger, *Surf. Interface Anal.*, 2014, **46**, 668–672.
61 A. Hennig, P. M. Dietrich, F. Hemmann, T. Thiele, H. Borcherding, A. Hoffmann, U. Schedler, C. Jäger, U. Resch-Genger and W. E. S. Unger, *Analyst*, 2015, **140**, 1804–1808.
62 A. F. Wagner, E. Walton, G. E. Boxer, M. P. Pruss, F. W. Holly and K. Folkers, *J. Am. Chem. Soc.*, 1956, **78**, 5079–5081.
63 E. A. Rusu, K. Magyari, L. Baia and M. Baia, *J. Mol. Struct.*, 2022, **1248**, 131501.

